Ti3SiC2-SiC multilayer thin films deposited by high temperature reactive chemical vapor deposition

Jorge Sanchez Espinoza, Fatma Trabelsi, Christophe Escape, Ludovic Charpentier, Marc Fivel, Elisabeth Blanquet, Frédéric Mercier

Ti3SiC2-SiC multilayer thin films deposited by high temperature reactive chemical vapor deposition

Jorge Sanchez Espinoza, Fatma Trabelsi, Christophe Escape, Ludovic Charpentier, Marc Fivel, Elisabeth Blanquet, Frédéric Mercier

PII: S0257-8972(22)00736-8

DOI: https://doi.org/10.1016/j.surfcoat.2022.128815

Reference: SCT 128815

To appear in: *Surface & Coatings Technology*

Received date: 12 May 2022

Revised date: 13 July 2022

Accepted date: 18 August 2022

Please cite this article as: J.S. Espinoza, F. Trabelsi, C. Escape, et al., Ti3SiC2-SiC multilayer thin films deposited by high temperature reactive chemical vapor deposition, *Surface & Coatings Technology* (2022), https://doi.org/10.1016/j.surfcoat.2022.128815

Ti_3SiC_2-SiC multilayer thin films deposited by High Temperature Reactive Chemical Vapor Deposition

Jorge Sanchez Espinoza[1], Fatma Trabelsi[1], Christophe Escape[2], Ludovic Charpentier[2], Marc Fivel[1], Elisabeth Blanquet[1], Frédéric Mercier[1]

[1]*Univ. Grenoble Alpes, CNRS, Grenoble INP, SIMaP, F-38000 Grenoble, France*

[2] *PROMES-CNRS, 66120 Font-Romeu Odeillo, France*

Abstract

Ti_3SiC_2-SiC multilayer film coatings synthesis was investigated with the high temperature reactive chemical vapor deposition technique. The method consists of a reaction between SiC (as the substrate and interlayers) and H_2 - $TiCl_x$ gaseous mixture. Cross-section morphologies and phases were studies by scanning electron microscopy (SEM), X-ray diffraction (XRD) and automated crystal orientation mapping in transmission electron microscopy (ACOM-TEM). Thermodynamic calculations were carried out to select more appropriate gas composition for reactor conditions and understand the chemistries of reaction between layers in the different steps. Nano and Vickers micro-indentation mechanical tests determined hardness and elastic modulus of the Ti_3SiC_2 and $Ti_5Si_3C_x$ surfaces samples. Oxidation tests and emissivity measurements allowed the evaluation of Ti_3SiC_2-SiC coatings as materials for high temperature applications. The multilayered systems kept their mechanical integrity and showed low degradation after 25 h of thermal cycles at 900 °C in air. The measurement of the optical properties also revealed an increase of the absorptivity after the oxidation of Ti_3SiC_2 surface sample.

Keywords

Titanium silicon carbide, MAX Phases, Chemical vapor deposition, Coatings, High temperature applications.

1 Introduction

The MAX phases, with the general formula $M_{n+1}AX_n$, where M is a transition metal, A one of the group A elements and where X can be carbon or nitrogen, have been reported as interesting compounds, given their unusual combination of useful physical properties such as high electrical and thermal conductivity, high tensile and compressive strength at high temperatures and good resistance to neutron irradiation [1-3]. Due to their unique set of properties, MAX phases could be very attractive for various industrial applications and in aggressive environment, such as materials for nuclear power plants, thermal barriers for aircraft engines, thermal shock resistant refractories or solar thermal energy receivers [2, 4-6].

Titanium silicon carbide (Ti_3SiC_2) is the most studied compound in the MAX phase family and the only one, which has been synthesized by chemical vapor deposition (CVD) to date. Most of the work in CVD of Ti_3SiC_2 was done by injecting simultaneously all the elements (Ti, Si and C) in the gas phase. This method has never given satisfactory results in order to obtain this MAX phase as single component, since it always coexists with small amounts of other solid phases such as TiC_x, $TiSi_2$, SiC, and $Ti_5Si_3C_x$ [7-10]. More recently, a method based on the reaction between a gas and a solid phase has been proposed by Jacques *et al.*, and allows deposition of Ti_3SiC_2 at 1100 °C [11]. In that technique, referred to reactive chemical vapor deposition (RCVD), a SiC film is deposited by classical CVD, followed by a step with a gas containing the Ti element. Then, Ti_3SiC_2 is formed by a reaction between the gas and the solid SiC. The process can be repeated in a sequential mode leading to a Ti_3SiC_2-SiC multilayer coating or a single component Ti_3SiC_2 coating if the SiC layer is totally converted. In 2008, Fakih *et al.* [8] showed thermodynamically that starting from the $SiC_{(s)} + H_{2(g)} + TiCl_{4(g)}$ system at 1100 °C, it was

possible to obtain a large equilibrium zone favoring the formation of $Ti_3SiC_{2(s)}$. Despite the existing literature, the development of chemical vapor deposition of Ti_3SiC_2 remains to be understood and controlled together with the evaluation of the properties in order to accelerate the transfer to the aforementioned applications.

In the present work, a variant of the RCVD technique is studied in which a solid surface ($SiC_{(s)}$) reacts with $TiCl_{x(g)}$ *in situ* produced, coming for the reaction of chloride gas passing over solid titanium pellets. The system is studied through a thermodynamic and experimental approach in order to investigate the appropriate fabrication parameters. Once the objective of manufacturing and replicability of the multilayer phases had been achieved, optical and mechanical properties tests were carried out, in order to determinate the feasibility to use this kind of materials for different applications.

2 Materials and Method

2.1 RCVD Experiment

Multilayer thin films were grown by high temperature reactive chemical vapor deposition (HT-RCVD). Prior to the HT-RCVD process, bulk polycrystalline SiC (Ferrotec-ADMAP, Japan) substrates were cut into small specimens with dimensions of approximately 15×15×0.3 mm. Before loading into the CVD reactor, these substrates were ultrasonically cleaned for 5 minutes in acetone, ethanol and isopropanol, successively. The HT-RCVD set-up consists of a graphite susceptor heated by induction in a vertical cold-wall reactor, which has been detailed previously [12, 13]. Briefly, the reactor consists of two zones. In the first zone, chlorine gas Cl_2 (99.99 %), was reacting with titanium (99.98%) solid pellets at 650 °C approx., to form a mixture of $TiCl_{x(g)}$ gases. These $TiCl_{x(g)}$ gases were then diluted in hydrogen and transported in the second zone where the $SiC_{(s)}$ substrates were placed on the susceptor. At the beginning of each run, substrates are heated up to the desired deposition temperature under the desired flow of $H_{2(g)}$. Then, the chlorine gas is injected in the desired proportion after five minutes of temperature stabilization. The total pressure inside the reactor was set to 2 kPa. The deposition temperature is fixed at 1300 °C and was measured inside the susceptor using an infrared pyrometer.

For this work, the ratio $R = [H_{2(g)}]/[TiCl_{x(g)}]$ was defined as the dilution ratio between hydrogen and titanium containing gases for the system. For the purposes of this work, the R value used is approximately R= 60, considering 390 sccm (standard cubic centimeter per minute) of H_2 and 10 sccm of Cl_2 gas flow, at operating conditions of the chlorinator in the reactor. In these conditions, no recirculation loops are observed in the gas phase, based on CFD calculations (not given here).

For multilayer experiments, the reactants used for $SiC_{(s)}$ layer were silane ($SiH_{4(g)}$ - 3% in H_2) 250 sccm and propane (C_3H_8) 5 sccm. A repetitive deposition sequence was designated as $(T\text{-}t'/S\text{-}s')_n$, were t´ is the time in minutes for each $Ti_xSi_yC_z$ (T) layer growth, s´ was the number of minutes used for each SiC (S) layer deposition, and n the total number of repeated sequences. The values for s′ and t′ vary between 1-10 min, and n between 1-3 cycles. An evacuation of reactive gases for 3 min was made between each deposited layer. After the growth, the samples were cooled down to room temperature at a rate of about 50 °C/min under $H_{2(g)}$ with a flow rate of 200 sccm. The experiments were performed in duplicate, obtaining equivalent characterizations between samples, indicating that the process is replicable.

The surface morphology and cross-sectional microstructure of as-grown $Ti_xSi_yC_{z(s)}$ - $SiC_{(s)}$ layers were characterized by scanning electron microscopy (SEM- JEOL IT500HR LV) and X-ray diffraction (XRD) analysis using a BRUKER D8 advanced diffractometer (SeriesII-2009) with Cu Kα radiation (λ=1.54 Å), Additionally, ACOM-TEM (automated crystal orientation mapping in transmission electron microscopy) was performed for the phase and orientation mapping with a resolution down to the nanometer scale (probe size of 1.6 nm) [14, 15]. The normal spectral reflectivity at 300 K was measured with a Perkin Elmer HDR 950 for the range 0.25 to 2.5 µm and with a SOC 100 HDR for the range 2.5 to 25 µm. All samples were considered as opaque, consequently the spectral emissivity ε(λ) is calculated from the spectral reflectivity as ε(λ) = 1-ρ(λ). We also consider the Kirchhoff law applies, so that the solar absorptivity (α) can be calculated from the measured spectral emissivity ε(λ) and the spectral solar irradiance I(λ) (using the reference Air Mass 1.5 Spectra [16]) according to (Eq 1). Total emissivity was obtained from the measured spectral hemispherical emissivity and the calculated

spectral blackbody emittance at 300 K, Ebb (λ, 300K) (Eq 2), according to Planck's law. The absorptivity to emissivity ratio (α/ε) was used to evaluate the spectral selectivity of materials.

$$\alpha(T) = \frac{\int_{0.}^{+\infty} \varepsilon(\lambda,\mathrm{T}) \cdot I(\lambda) \cdot d\lambda}{\int_{0}^{+\infty} I(\lambda) \cdot d\lambda} \approx \frac{\sum_{0}^{N-1} \varepsilon(\lambda_n,\mathrm{T}) \cdot I(\lambda_n)\,(\lambda_{n+1}-\lambda_n)}{\sum_{0}^{N-1} I(\lambda_n)\,(\lambda_{n+1}-\lambda_n)} \quad (1)$$

$$\varepsilon(T) = \frac{\int_{0}^{+\infty} \varepsilon(\lambda,\mathrm{T}) \cdot E_{bb}(\lambda,T) \cdot d\lambda}{\int_{0}^{+\infty} E_{bb}(\lambda,T) \cdot d\lambda} \approx \frac{\sum_{0}^{N-1} \varepsilon(\lambda_n,\mathrm{T})\, E_{bb}(\lambda_n,\mathrm{T})\,(\lambda_{n+1}-\lambda_n)}{\sum_{0}^{N-1} E_{bb}(\lambda_n,\mathrm{T})\,(\lambda_{n+1}-\lambda_n)} \quad (2)$$

For the nano-indentation tests, a set of 25 indents using Berkovich indenter were performed on the as-grown surface of samples in a two-dimensional array (x- and y- spacing distance of 10 µm) with a load of 50 mN and holding time of 10 s before unloading. The hardness and Young's modulus were extracted from the load-penetration depth (displacement) data using the Oliver and Pharr method.

2.2 Thermodynamic modeling

Thermodynamic modeling in the Ti-Si-C-Cl-H system was made using FACTSAGE [17] + FactPS database software package (version 7.3) and complemented with data coming from the work of Du *et al* [18]. The computation was made by the minimization of the Gibbs free energy of the whole chemical system. Firstly, the ternary system Ti-Si-C was studied at 1300 °C and 1 bar. Then the $H_{2(g)}$ + $TiCl_{3(g)}$ + $SiC_{(s)}$ system was calculated in order to evaluate the effect of dilution ratio on the formation of solid species.

3 Results and Discussion

3.1 Thermodynamic Results

The ternary Ti-Si-C phase diagram system calculated at 1300 °C and 1 bar is presented in Figure 1 (a). Ti_3SiC_2, which is a defined compound, is in equilibrium with different phases TiC_x, SiC, $Ti_5Si_3C_x$ and $TiSi_2$. The isothermal section is similar to those previously reported in the literature for 1100 °C [18, 19]. For the experimental system proposed, it is important to first describe the phenomena inside the chlorinator. As a precedent to this, Tsavdaris *et al.* [20] analyze that over 650 °C, the chlorine quickly reacts with the solid titanium pellets forming a layer of $TiCl_{2(s)}$ over it, which continues to react with $Cl_{2(g)}$. The main species produced as a function of the chlorination temperature are $TiCl_{3(g)}$ and $TiCl_{4(g)}$ in almost the whole studied range (600 – 1200 °C) with a strong predominance of $TiCl_{3(g)}$ over 750 °C (more than 90 at %). No unreacted $Cl_{2(g)}$ remains at the chlorinator outlet. For that reason, a ternary $SiC_{(s)}$ -$H_{2(g)}$ -$TiCl_{3(g)}$ phase diagram system was calculated at 1300 °C and 2 kPa, presented in Figure 1 (b). With this system, it is possible to establish a quite wide zone favorable –filled up in green- to the formation of $Ti_3SiC_{2(s)}$, even larger than with $TiCl_{4(g)}$ system [8]. To understand the role of the dilution ratio R = $[H_{2(g)}]/[TiCl_{3(g)}]$, two equilibrium calculations were made for a solid surface reactive of a given amount of 1 mol SiC - kept constant-, varying the number of moles (n) $TiCl_{3(g)}$ between 10^{-1}-10^{2} mol for R=1 (Figure 2 (a and c)) and R=100 (Figure 2 (b and d)) at 1300 °C and 2 kPa. Proportionally; $H_{2(g)}$ mole number is multiplied by R*n and the volume by n. This type of calculation gives the influence of dilution (when looking to the effect of different values of R) and amount of active gases ($H_{2(g)}$, $TiCl_{3(g)}$) *vs* solid SiC (when looking to the effect of n).

For small dilution ratio (Figure 2 (a)), the amount of solid SiC versus $TiCl_{3(g)}$ has a strong effect on the solid phases formed. In the left of the diagram, when the amount of $SiC_{(s)}$ is in excess, the solid phases at equilibrium are just Ti_3SiC_2 and in a less extent TiC_x. On the other hand, when $SiC_{(s)}$ is less available, production of the solid MAX phase Ti_3SiC_2 begins to reduce and convert, as the amount of $TiCl_{3(g)}$ gas increases, into the $Ti_5Si_3C_x$ and then TiC_x phases. For higher dilution ratio (Figure 2 (b)), it is observed that when SiC is available in the system, the formation of Ti_3SiC_2 and in a lesser extent $TiSi_2$ is favored. However, as the concentration of $TiCl_{3(g)}$ increases, production of the solid MAX phase Ti_3SiC_2 begins to reduce and convert into the TiC_x and $Ti_5Si_3C_x$ phases. Furthermore, if the equilibrium calculations for the gas phases are observed (Figure 2 (c) and (d)), it is clear that the SiC substrate contributes to species present in the gas phase. The silicon containing species are mainly $SiCl_{2(g)}$ and $SiCl_{3(g)}$, and when the availability of these gases begins to be reduced, changes in the configuration of the solid phases occur. On the other hand, no carbon containing gas phases are observed and all the carbon participate to the solid phase with the formation of Ti_3SiC_2, $Ti_5Si_3C_x$ or TiC_x (Figure 2 (a) and (b)). The formation of Ti_3SiC_2 can therefore be interpreted as the following: the silicon is coming from chlorosilanes produced by the reaction of SiC with the $H_{2(g)} + TiCl_{x(g)}$ gas mixture, while the carbon is coming through the diffusion in the growing Ti_3SiC_2. Once the substrate is covered with an increasingly thick layer of Ti_3SiC_2, the Si contribution to the system from the substrate is reduced, only now through solid-phase diffusion from the SiC substrate to the formed Ti_3SiC_2 layer, therefore the $H_{2(g)} + TiCl_{x(g)}$ gas mixture begins to react with the MAX phase, changing the conditions, shifting the equilibrium towards the favorable zone of production of $Ti_5Si_3C_x$ phase primarily.

As a conclusion of this part, from the titanium chlorination procedure and through the proposed experimental setup, it was possible to produce the MAX phase Ti_3SiC_2 by RCVD at 1300°C. In

addition, SiC must be supplied if the appearance of other phases such as TiC_x, $Ti_5Si_3C_x$ and $TiSi_2$ is to be avoided, given the strong dependence on the amount of SiC available during the process for the formation of only Ti_3SiC_2, something that can be achieved in the reactor by the fabrication of successive SiC layers.

3.2 Experimental Results

From the previous section, it is clear that in order to prioritize the formation of the MAX phase $Ti_3SiC_{2(s)}$ for the presented system, it is necessary to work with a high gas ratio R, sufficiently diluted to prevent the formation of TiC_x, but taking into account that on the other hand, a very high R favors the formation of $TiSi_2$ to the detriment of the MAX phase at 1300°C. Therefore, test experiments were initiated at different temperatures (1100-1300 °C) and gas ratios, obtaining favorable results in order to fabricate the MAX phase Ti_3SiC_2. The experiments presented below were all made at temperature of 1300 °C, pressure of 2 kPa and with a gas ratio of approximately R= 60 (considering a gas production of 90% $TiCl_{3(g)}$ and 10% $TiCl_{4(g)}$ from chlorination process). These conditions were found experimentally and were the best conditions in the range investigated to observe reactivity between $SiC_{(s)}$ and $TiCl_{x(g)}$-$H_{2(g)}$ mixtures.

3.2.1 One-Layer deposition (A)

A 10-minute $(T\text{-}10')_1$ HT-RCVD experiment -labeled sample A- was made under the conditions presented previously. A SEM characterization in the cross section was carried out to observe the morphology of the reaction zone between $SiC_{(s)}$ and the gas mixture. Figure 3 (a) show columnar grains (0.7-µm length approx.) in the middle zone, characteristics of the MAX phase Ti_3SiC_2. In addition to this phase, XRD analysis confirms also the presence of $Ti_5Si_3C_x$. According to the results presented, it is possible to confirm a correlation between the thermodynamic and the

experiment results, in relation to the ratio of the gases and the solid phases obtained, where high dilution of $TiCl_{x(g)}$ in hydrogen gas, favors the formation of the Ti_3SiC_2 accompanied with $Ti_5Si_3C_x$ phases. Additionally, the ACOM-TEM observation (Figure 3 (b)) shows that the result of the experiment consists of three dense and well-defined layers, starting with the SiC substrate, then the MAX phase Ti_3SiC_2 and finally the $Ti_5Si_3C_x$ phase on the surface. The absence of TiC_x phase is confirmed. Orientation mapping reveal polycrystalline layers with no preferential orientation (Figure 3 (c)).

It can be noted that with this experimental procedure, it is not possible to achieve the control of the amount of SiC available in solid phase on the surface during the process. In order to reduce the other titanium phases, the system must be fed with SiC layers to be consumed, between the Ti_3SiC_2 deposition layers in order to obtain a single component Ti_3SiC_2 MAX phase. For that purpose, the sequential synthesis of SiC and Ti_3SiC_2 layers was investigated.

3.2.2 Bi-layer deposition (B)

A bi-layer coating (T- 10′/ S-10′/)$_1$ with a total thickness of about 5 µm was deposited by repeating the procedure used for the previous deposit (A) followed by a 10 minute injection of 250 sccm of silane (3% in H_2) and 5 sccm of propane gas flow (C/Si =2), for SiC deposition. The XRD pattern (Figure 4) indicates the presence of four phases: SiC, Ti_3SiC_2, $Ti_5Si_3C_x$ and $TiSi_2$. Also Figure 5 shows a cross section, where it is possible to identify again the columnar grains in the first sublayer, in addition, a growth of the deposition area of titanium-containing phases is observed, which is explained by the interaction of the top SiC layer at the interface with Ti_5SiC_x phase. Its formation is discussed below.

3.2.3 Multilayer deposition (C)

For the multilayer deposition, a sequence: (T- 5′/ S-5′/)$_1$ - (T- 3′/ S-1′/)$_2$ -(T- 3′)$_1$, with a total thickness of about 6 μm was deposited, where the deposition times were reduced for both titanium-containing and SiC phases, looking for the highest purity of the MAX phase. The final layer is Ti_3SiC_2. Figure 6 (a) shows a cross section of the deposition, where it is possible to see how the last three layers of columnar grains between the SiC deposits present the characteristic morphology of the MAX Phase Ti_3SiC_2. In addition, a grazing incidence XRD (angle of incidence - 1.1°) characterization was made, to increase the response of the surface layer, obtaining as a result the increase of the peaks of the main phase Ti_3SiC_2 (two other $TiSi_2$ and Ti_5SiC_x phases were possibly formed only in the first layer since it had a deposition time of 5 min (T-5')). Additionally, the cross-section observed with the ACOM-TEM technique (Figure 6 (b)) for (T- 3′/ S-1′/)$_2$ -(T- 3′)$_1$ depositions layers reveals no traces of secondary Ti phase, and confirms the single component Ti_3SiC_2 between the SiC interlayers. All the grains are well crystallized in the MAX phase. All the layers are dense without porosity in the limit of the samples observed. Furthermore, the grain size varies between 0.3-0.7 μm for Ti_3SiC_2 phase and below 50 nm for SiC. Finally, all the layers are polycrystalline without preferential orientation (Figure 6 (c)).

3.3 Discussion

In order to summarize and complement the experimental study, a deposition diagram of the experiments is presented in Figure 7. From a SiC substrate, after 10 minutes of deposition (experiment A) two titanium phases are obtained, Ti_3SiC_2 and $Ti_5Si_3C_x$. Fakih *et al.* [21] observed that a critical deposition time exists above which Ti_3SiC_2 coexists with $Ti_5Si_3C_x$. Below this critical time, only Ti_3SiC_2 exists. This critical time can be seen as the limit to keep enough Si containing gaseous species in the gas phase (mainly $SiCl_{2(g)}$ and $SiCl_{3(g)}$) just above the surface

in order to favor the formation of Ti_3SiC_2. Based on the multilayers experiments, we estimate this time to 3 minute in our conditions. The delicate balance between gaseous species ($TiCl_x$ and $SiCl_x$) explain why all the attempts of classical CVD failed to achieve single component Ti_3SiC_2. Following this first reaction between $SiC_{(s)}$ and $TiCl_{x(g)}$-$H_{2(g)}$ mixture, two scenarios are possible. First, if $Ti_5Si_3C_x$ is formed, its reaction with the growing SiC leads to the formation of additional phases since these two compounds are not in equilibrium (Figure 1 (a)). Thermodynamic equilibrium calculation was performed between 1 mol of SiC +1 mol of $Ti_5Si_3C_x$ at 1300° C and 2 kPa, and the results indicate the formation of 0.11 mol of Ti_3SiC_2 and 0.77 mol of $TiSi_2$ in agreement with the experimental results (sample B), in terms of the occurrence of the $TiSi_2$ phase. Alternatively, if $Ti_5Si_3C_x$ is not formed (reaction time below 3 minutes), the growth of Ti_3SiC_2-SiC multilayers is possible since these two compounds are in equilibrium. If the SiC deposition time is further reduced, a dense Ti_3SiC_2 layer could be obtained as it was demonstrated by Fakih *et al* [21].

3.4 Mechanical Tests

In order to determine the mechanical properties of the samples (A and C), nano- and micro-indentation tests were performed on two different zones of the samples surface. The first zone was defined close to the top of the film where only the $Ti_5Si_3C_x$ phase is present. Three indentations tests, for the sample A, were performed which gave average hardness and Young's modulus values of 11-13 GPa and 230 GPa respectively. These values for the hardness and elastic modulus are in good agreement with what is reported in literature for the $Ti_5Si_3C_x$ phase [22]. The second zone is defined much deeper in the film, estimated at 660 nm from the top, where a mix of $Ti_5Si_3C_x$ and Ti_3SiC_2 phases are supposed to be present. Twenty-two indentations were realized. It is found that the average hardness decreases to 4-5.3 GPa. This decrease is

probably related to the presence of numerous grain boundaries. Residual imprints of the indents were not detected by optical microscopy nor by SEM.

For sample C, the average hardness and Young s modulus were measured as 0.29 GPa and 30 GPa respectively, at a penetration depth of 270 and 470 nm. For the two samples (A and C), no residual impression was detected for the matrix after nano-indentation. The indentation response at this load is almost entirely elastic. For this reason, it was decided to change to a micro-indentation test for the sample C. Different charges were applied in order to identify the residual impression of the indents and measure the diagonals of the Vickers indent. The average lengths of the two orthogonal diagonals were determined from SEM observations and converted to hardness values using the standard Vickers hardness (HV) formula:

$$HV = 1.854 * (F/d2) \quad (3)$$

Where F is applied load and d the average of two diagonals. It was found that at low loads less than 0.5 N, the indents print cannot be clearly detected with optical microscope nor SEM. At the load of 0.5 N the average hardness measured for the film was 27.6 GPa. With increasing the load to 1 N, the hardness decreased to 24 GPa, this decrease means it was indented mostly Ti_3SiC_2 phase and not a mix of Ti_3SiC_2 + SiC phases. This values are in agreement with the work of Emmerlich *et al* [23]. Meanwhile, the surface around the indent in Figure 8 reveals no pileup and no deformation despite the large indentation load.

3.5 Optical properties at room temperature

The coatings were all processed as presented above, on polycrystalline SiC samples. Figure 9 presents the normal spectral emissivities of SiC coated by A, B, and C before (a) and after

oxidation (b) of 25 h at 900°C in air at ambient pressure in a Nabertherm P310 tube furnace equipped with an alumina tube (Sceram ceramics). After each oxidation cycle (6 cycles during the 25 h), the samples are taken out from the furnace and cooled down to room temperature in air. Interestingly, all the samples kept their structural integrity through the cyclic oxidation and no cracks were detected under optical microscope. Interference fringes are observed due to the semi-transparence of SiC [24]. For oxidized samples, a peak at 10 µm is clearly visible. This peak is attributed to TiO_2 rutile [24]. A drop of emissivity is noticed on oxidized samples that could be attributed to the formation of silica [24]. Table 1 reports the values of the solar absorptivity, total emissivity and α/ε ratio calculated for A, B and C samples from the integrated values of spectral emissivity, using eq. (1) and (2), before and after oxidation. It is observed from Table 1 that the MAX Phase coating (C experiment) presents the best result for the three samples evaluated in terms of ratio (α/ε) before oxidation. Also in those three samples, the solar absorptivity is improved after oxidation cycle. The optical properties of the B coated are less affected by the cyclic oxidation, even increased the value α/ε ratio from 1.86 to 2.4. In summary, Ti_3SiC_2 MAX phase coating material presents interesting prospects as a material for optical applications, something in agreement with the results reported by Li *et al.* [25, 26]. Further studies are necessary to evaluate the performance of these materials in terms of emissivity and absorptivity at high temperatures.

4 Conclusion

Based on the thermodynamically results, it was established that growth of MAX phase Ti_3SiC_2 is possible through the reaction of $TiCl_{x(g)}/H_{2(g)}$ mixture on SiC surface, in the conditions presented with the chlorination method. Experimentally, the growth of Ti_3SiC_2 layers on SiC substrates was achieved at 1300 °C by HTRCVD. The average growth rate of polycrystalline layers obtained at high temperature was about 14 μm h^{-1} for Ti_3SiC_2 (considering 0.7 μm in 3 min) and 20 μm h^{-1} for SiC. With this HT-RCVD multilayer experiment procedure, it is possible to control the thickness and type of coatings to be formed, even achieving the MAX phase Ti_3SiC_2 on surface.

Mechanical tests by nano- and Vickers micro-indentation suggest that the sample with the MAX phase on the surface exhibits good ductility and also high fracture toughness, with values between 24 and 27.6 GPa for hardness and no pile-up or deformation after indentation loading.

The multilayered systems depositions showed low degradation after thermal cycles at 900 °C in air for 25 h. For the sample with Ti_3SiC_2 finished surface, the measurement of the normal spectral emissivity also revealed an increase in the absorptivity after oxidation.

Acknowledgements

The authors want to thank the *Agence Nationale de la Recherche* (National Agency for Research) of the French State under awards ANR-17-CE08-0028 MAD_Ceramics and the Chilean National Commission for Scientific and Technological Research (*CONICYT*) for supporting the development of this study. The authors also would like to thank S. Coindeau and T. Encinas for the X-ray measurements and G. Renou for the ACOM-TEM acquisition. The optical measurements were supported by the French "Investments for the future" program managed by the National Agency for Research under contract ANR-10-EQPX-49-SOCRATE.

Bibliography

1. Barsoum, M. and T. El-Raghy, *The MAX Phases: Unique New Carbide and Nitride Materials.* American Scientist, 2001. **89**(4): p. 334.
2. Yoo, H.-I., M. Barsoum, and T. El-Raghy, *Ti_3SiC_2 has negligible thermopower.* Nature, 2000. **407**(6804): p. 581-582.
3. Barsoum, M., et al., *Thermal properties of Ti_3SiC_2.* Journal of Physics and Chemistry of Solids, 1999. **60**(4): p. 429-439.
4. Hoffman, E., et al., *MAX phase carbides and nitrides: Properties for future nuclear power plant in-core applications and neutron transmutation analysis.* Nuclear Engineering and Design, 2012. **244**: p. 17-24.
5. Le Flem, M., et al., *Irradiation damage in Ti_3 (Si, Al) C_2: a TEM investigation.* International Journal of Applied Ceramic Technology, 2010. **7**(6): p. 766-775.
6. Sundberg, M., et al., *Alumina forming high temperature silicides and carbides.* Ceramics International, 2004. **30**(7): p. 1899-1904.
7. Racault, C., F. Langlais, and C. Bernard, *On the chemical vapour deposition of Ti_3SiC_2 from $TiCl_4$-$SiCl_4$-CH_4-H_2 gas mixtures.* Journal of materials science, 1994. **29**(19): p. 5023-5040.
8. Fakih, H., et al., *Phase Equilibria and Reactive Chemical Vapor Deposition (RCVD) of Ti_3SiC_2.* Journal of Phase Equilibria and Diffusion, 2008. **29**(3): p. 239-246.
9. Goto, T. and T. Hirai, *Chemically vapor deposited Ti_3SiC_2.* Materials Research Bulletin, 1987. **22**(9): p. 1195-1201.
10. Pickering, E., W.J. Lackey, and S. Crain, *CVD of Ti_3SiC_2.* Chemical Vapor Deposition, 2000. **6**(6): p. 289-295.
11. Jacques, S., H. Fakih, and J.-C. Viala, *Reactive chemical vapor deposition of Ti_3SiC_2 with and without pressure pulses: Effect on the ternary carbide texture.* Thin Solid Films, 2010. **518**(18): p. 5071-5077.
12. Boichot, R., et al., *Epitaxial and polycrystalline growth of AlN by high temperature CVD: Experimental results and simulation.* Surface and Coatings Technology, 2010. **205**(5): p. 1294-1301.
13. Claudel, A., et al., *Thermodynamic and experimental investigations on the growth of thick aluminum nitride layers by high temperature CVD.* Journal of Crystal Growth, 2009. **311**(13): p. 3371-3379.
14. Valery, A., *Caractérisation de microtextures par la technique ACOM-TEM dans le cadre du développement des technologies avancées en microélectronique*. 2017, Université Grenoble Alpes (ComUE).
15. Rauch, E.F., et al., *Automated nanocrystal orientation and phase mapping in the transmission electron microscope on the basis of precession electron diffraction.* Zeitschrift für Kristallographie, 2010. **225**(2-3): p. 103-109.
16. (ASTM), *Reference Solar Spectral Irradiance: Air Mass 1.5, American Society for Testing and Materials (ASTM) (last access on april, 2022),.* USA, 2022: p. http://rredc.nrel.gov/solar/spectra/am1.5/.
17. *Factsage.* 2019. **V 7.3**: p. https://www.factsage.com/.
18. Du, Y., et al., *Experimental investigation and thermodynamic calculation of the titanium–silicon–carbon system.* Journal of the American Ceramic Society, 2000. **83**(1): p. 197-203.
19. Jacques, S., et al., *Pulsed reactive chemical vapor deposition in the C-Ti-Si system from H_2/$TiCl_4$/$SiCl_4$.* Thin Solid Films, 2005. **478**(1-2): p. 13-20.

20. Tsavdaris, N., et al., *A Chemical Vapor Deposition Route to Epitaxial Superconducting NbTiN Thin Films.* Chemistry of Materials, 2017. **29**(14): p. 5824-5830.
21. Fakih, H., et al., *The growth of Ti_3SiC_2 coatings onto SiC by reactive chemical vapor deposition using H_2 and $TiCl_4$.* Surface and Coatings Technology, 2006. **201**(6): p. 3748-3755.
22. Zhang, F., et al., *Effect of annealing temperature on microstructure and mechanical properties of plasma sprayed TiC-Ti_5Si_3-Ti_3SiC_2 composite coatings.* Surface and Coatings Technology, 2021. **422**: p. 127581.
23. Emmerlich, J., et al., *Growth of $Ti_3 SiC_2$ thin films by elemental target magnetron sputtering.* Journal of Applied Physics, 2004. **96**(9): p. 4817-4826.
24. Touloukian, Y. and D. DeWitt, *Thermophysical properties of matter-The TPRC data series. Volume 8. Thermal radiative properties-nonmetallic solids*. 1972, THERMOPHYSICAL AND ELECTRONIC PROPERTIES INFORMATION ANALYSIS CENTER , Databook, United States
25. Li, S., et al., *Optical properties of Ti_3SiC_2 and Ti_4AlN_3.* Applied Physics Letters, 2008. **92**(22): p. 221907.
26. Berger, O., *The correlation between structure, multifunctional properties and application of PVD MAX phase coatings. Part I. Texture and room temperature properties.* Surface Engineering, 2020. **36**(3): p. 225-267.

Tables

Table 1: Calculated values (Eqs. (1) And (2)) of the solar absorptivity, total emissivity and ratio α/ε for SiC coated with A, B, C deposition, before and after oxidation.

		HT-RCVD deposition			Oxidized 25 h in air at 900 °C		
	Surface	α	ε	α/ε	α	ε	α/ε
A	$Ti_5Si_3C_x$	0.48	0.16	3.06	0.83	0.57	1.46
B	SiC	0.74	0.40	1.86	0.86	0.36	2.40
C	Ti_3SiC_2	0.53	0.04	13.31	0.78	0.37	2.14

List of figures captions

Figure 1: Thermodynamic calculations at 1300 °C, (a) Ti-Si-C phase diagram isothermal section. (b) Deposition diagram applicable to the formation of RCVD coatings by reaction between a given amount (1 mol) of solid $SiC_{(s)}$ and a $H_{2(g)}$ + $TiCl_{3(g)}$ gaseous mixture at a total gas pressure of 2 kPa.

Figure 2: Calculated quantities of solid (a-b) and gaseous (c-d) species produced at equilibrium from the reaction of 1 mol SiC, $TiCl_{3(g)}$ between 10^{-1}-10^{2} mol, and R=1 (a and c) R=100 (b and d) , at 1300 °C and 2 kPa.

Figure3: Experiment characterization $(T\text{-}\ 10')_{1.}$ (a) SEM observation of cross section. (b) ACOM-TEM phase map. c) Orientation map of sample A.

Figure 4: XRD pattern of experiment B, produced by RCVD at 1300 °C, R = 60 and total gas pressure: 2 kPa.

Figure 5: SEM observation of experiment B in cross-section.

Figure 6: Multilayer experiment C. (a) SEM observation of cross section produced by RCVD at 1300 °C, R = 60 and total gas pressure: 2 kPa. b) Phase map with the ACOM-TEM technique. c) Orientation map with the ACOM-TEM technique. (Images b and c only show the six topmost layers).

Figure 7: Possible scenario of phase formation in the Ti-Si-C system by the RCVD technique.

Figure 8: Micro- indenter images in surface experiment C, for charge applied: 0.5 N and 1 N.

Figure 9: Evolution of the normal spectral emissivity at 300 K (a) HT-RCVD samples (b) oxidized 25 h at 900 °C

Figures

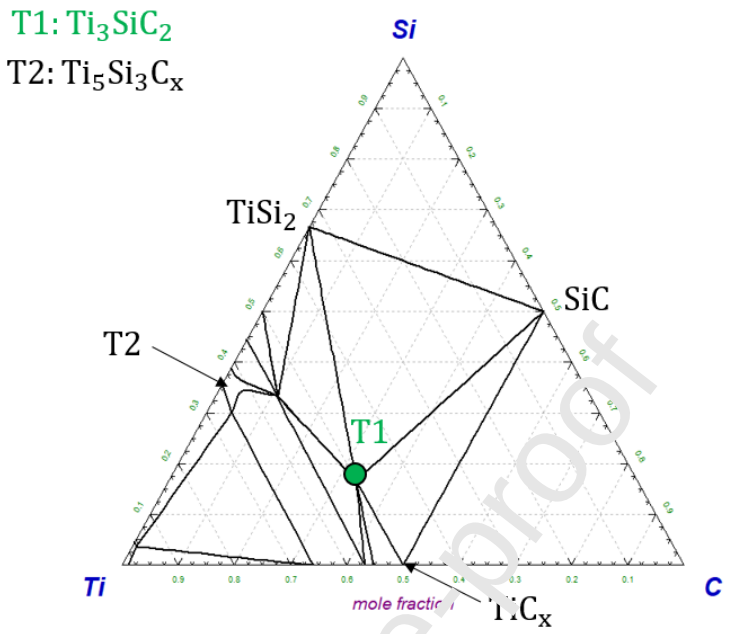

(a)

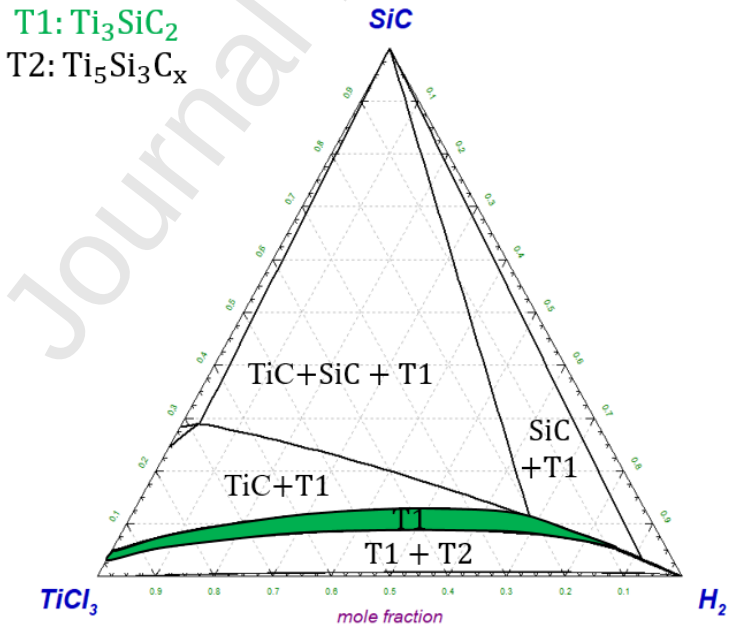

(b)

Figure 1

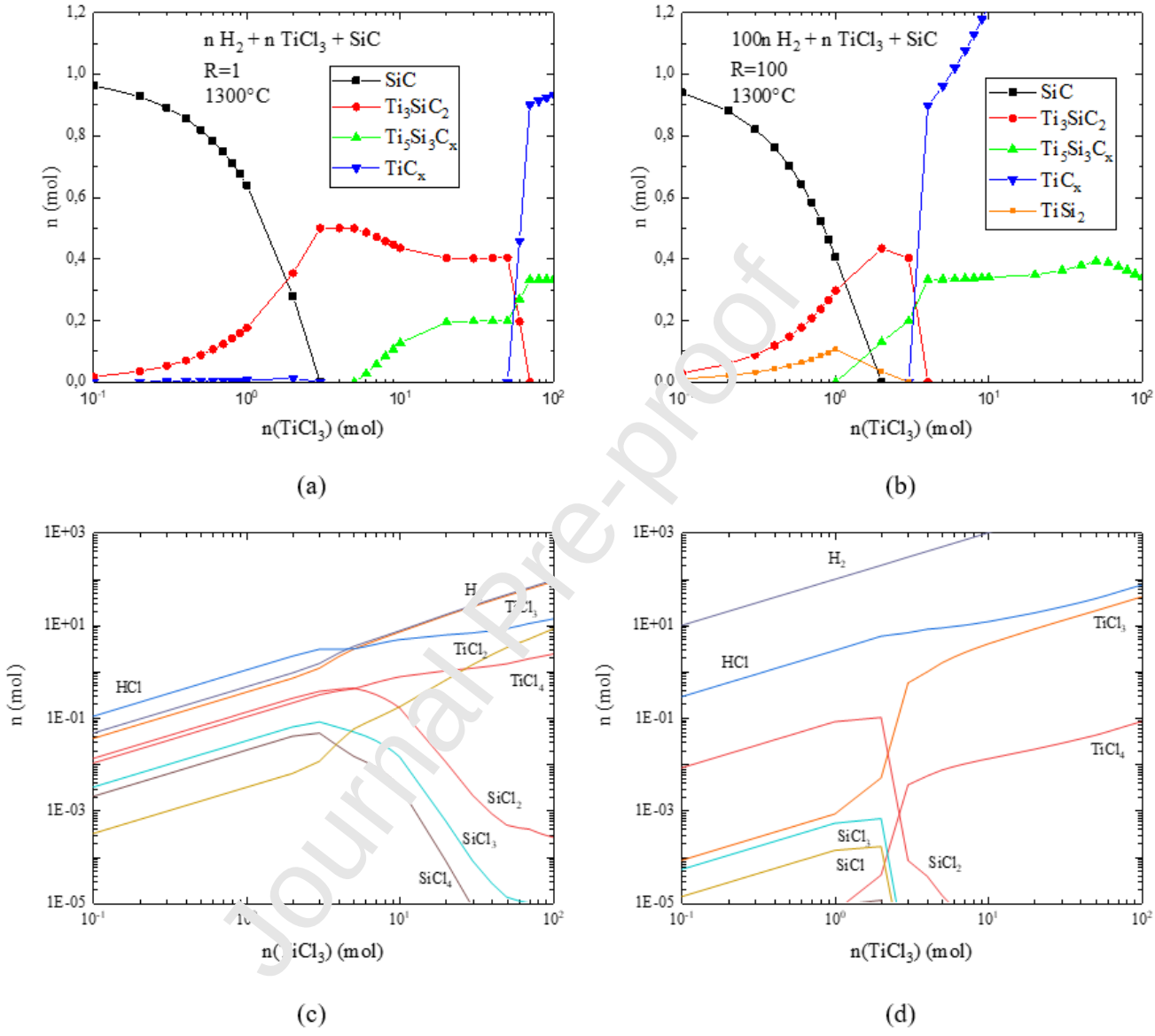

Figure 2

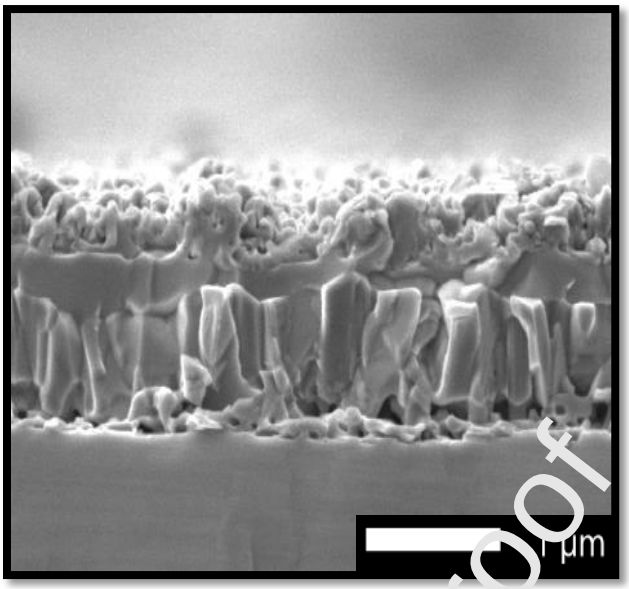

(a)

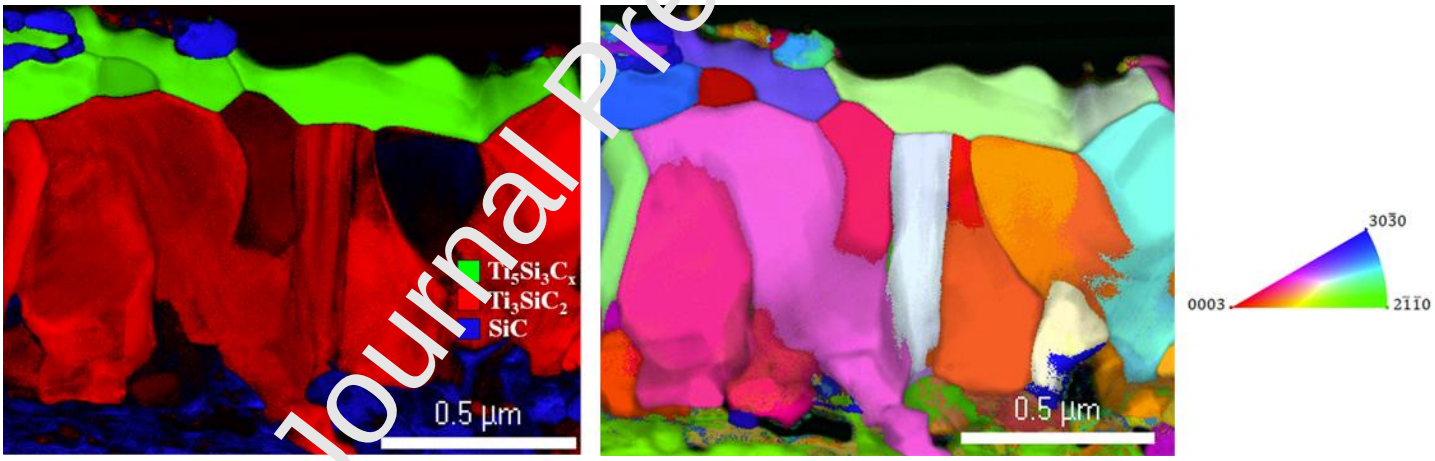

(b) (c)

Figure 3

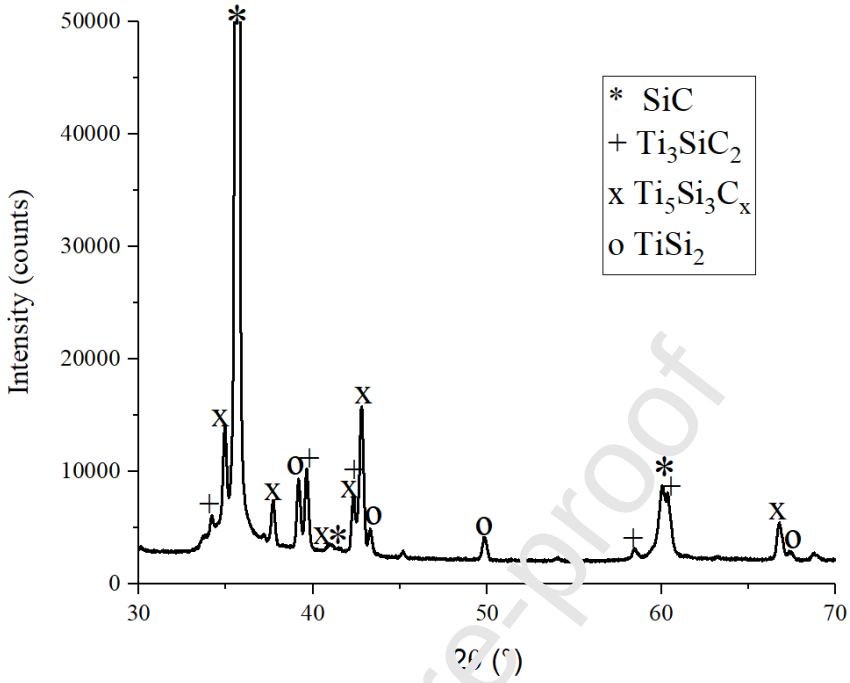

Figure 4

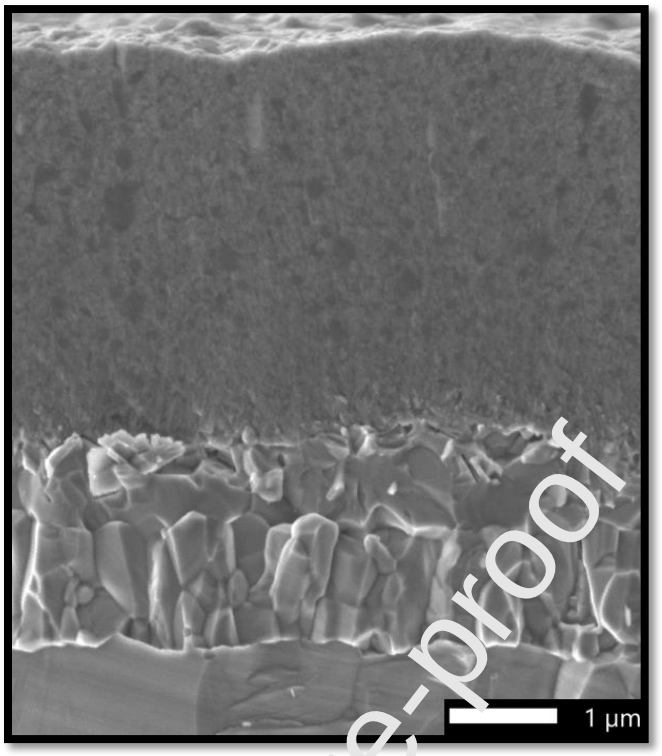

Figure 5

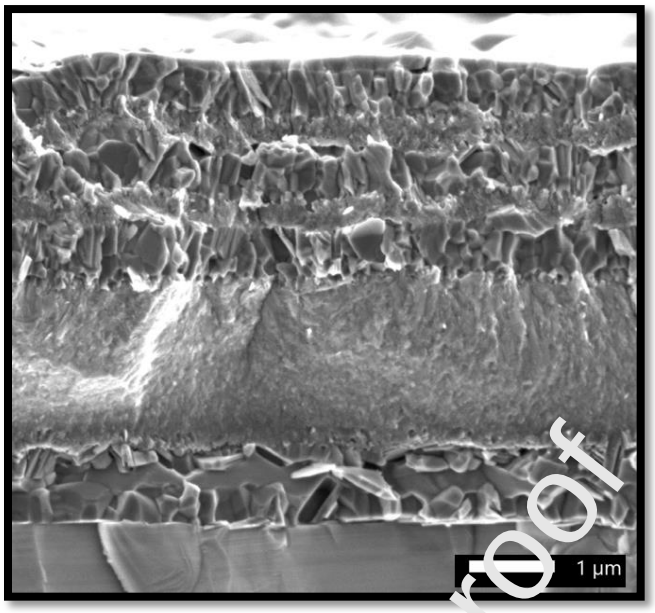

(a)

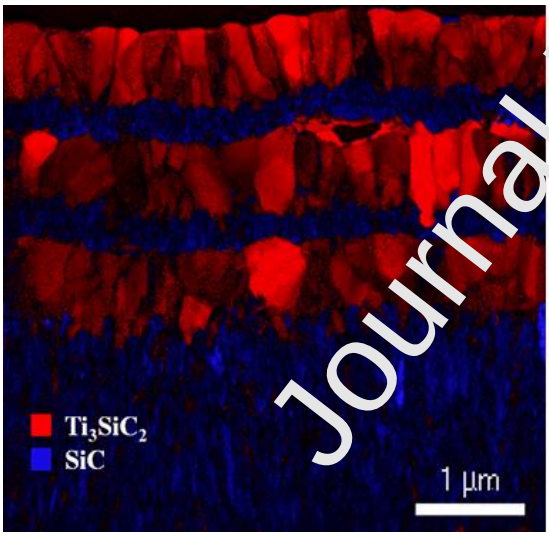

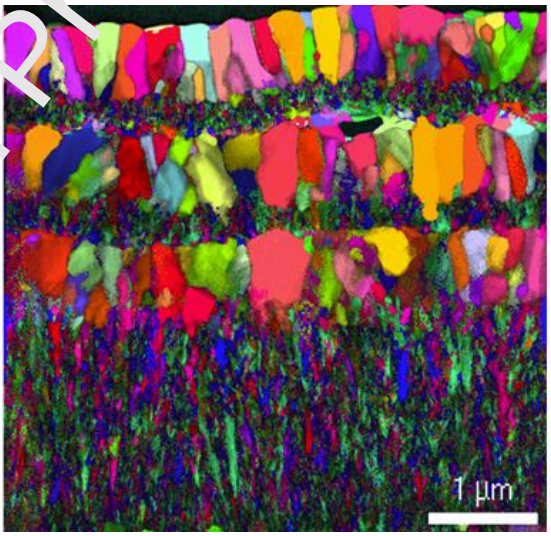

(b) (c)

Figure 6

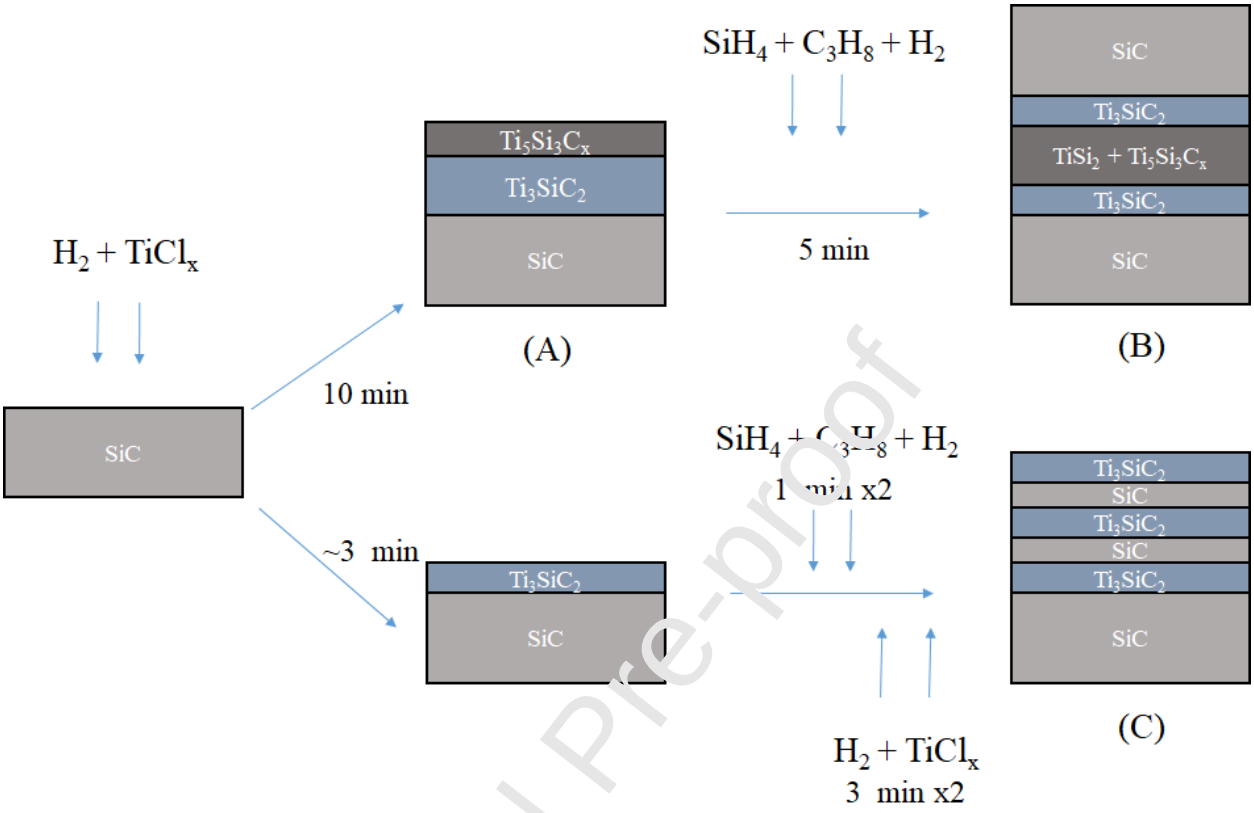

Figure 7

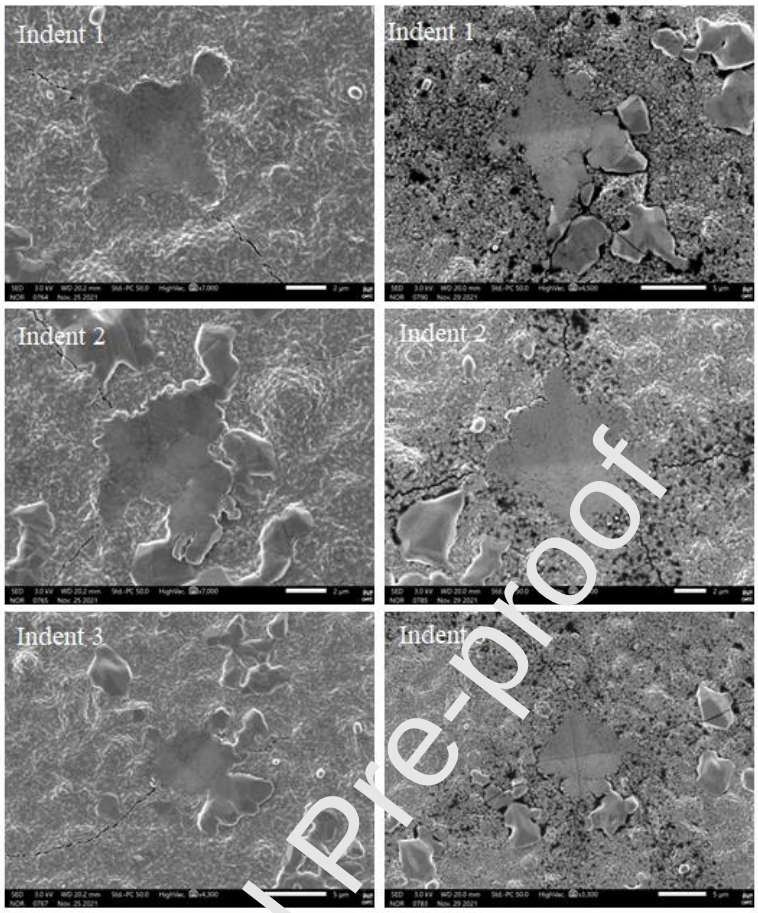

(a) Charge applied : 0.5 N (b) Charge applied : 1N

Figure 8

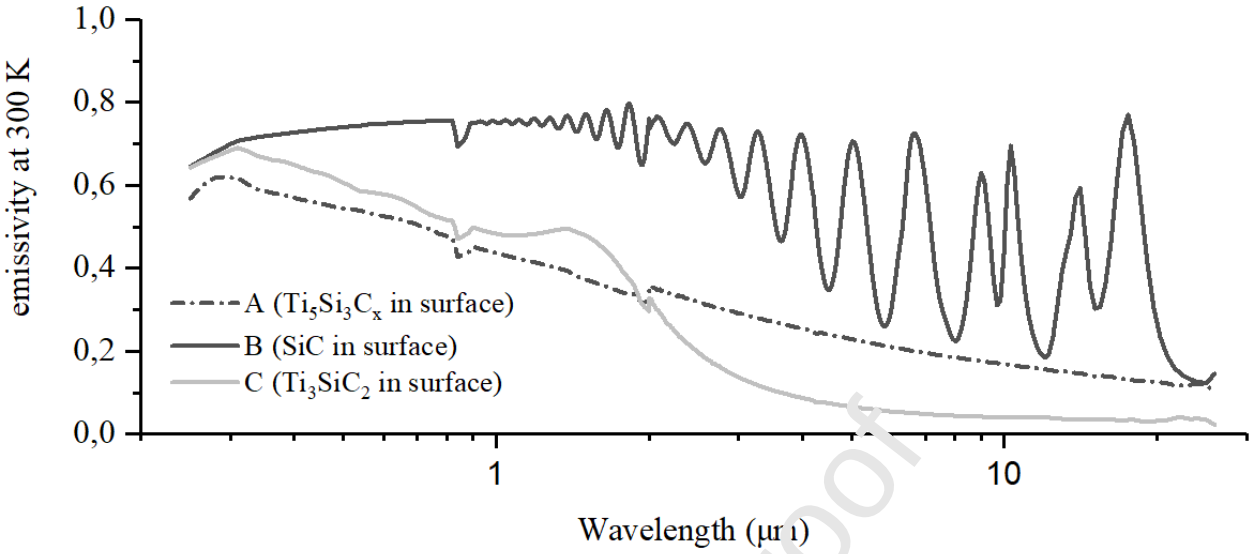

(a)

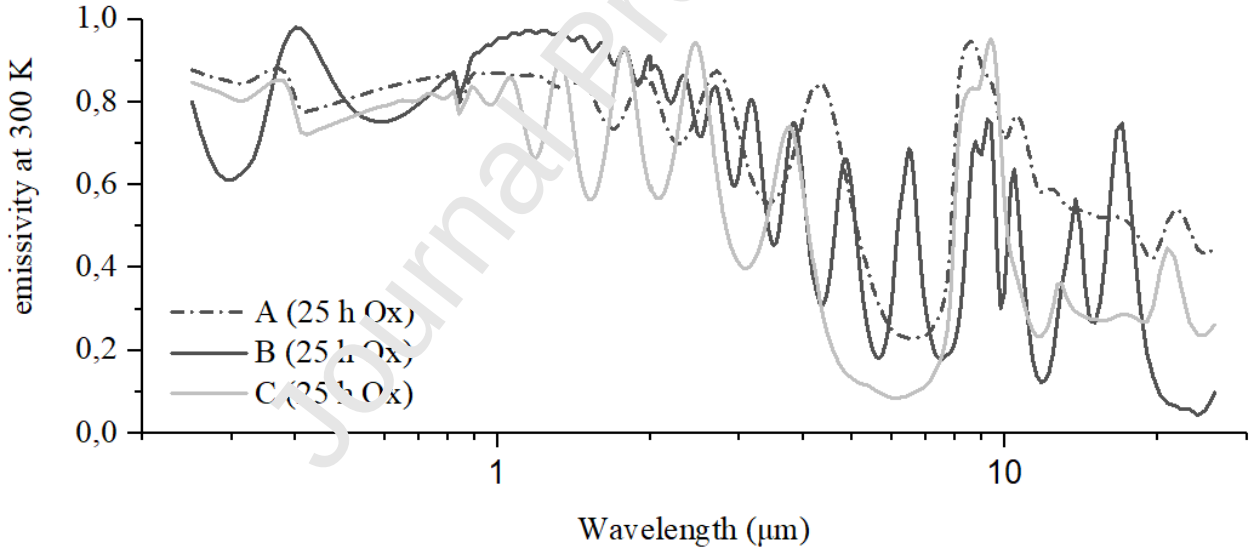

(b)

Figure 9

Highlights

-Phase formation and multilayer structure can be controlled in the Ti-Si-C system with the Reactive Chemical Vapor Deposition technique.

-Phase and orientation mapping down to the nanometer scale prove the synthesis of pure polycrystalline Ti_3SiC_2.

-ductility of Ti_3SiC_2 RCVD films at room temperature with no pileup or deformation after indentation loading.

-Ti_3SiC_2/SiC multilayers keep their integrity after thermal cycles at 900°C in air for 25 h Increase in the absorptivity after oxidation of Ti_3SiC_2 at 900°C.

Declaration of interests

☒The authors declare that they have no known competing financial interests or personal relationships that could have appeared to influence the work reported in this paper.

☐The authors declare the following financial interests/personal relationships which may be considered as potential competing interests:

CRediT authorship contribution statement

J. Sanchez: Methodology, CVD experiments, characterizations, writing – original draft, writing – review & editing. F. Trabelsi: Mechanical characterizations, writing – review & editing L. Charpentier: Optical characterizations, review & editing. Mark Fivel: Mechanical characterizations, review & editing. E. Blanquet: Conceptualization, writing-review & editing. C. Escape: Optical characterizations, review & editing. F. Mercier: Conceptualization, methodology, writing-original draft, writing – review & editing.